Design of fluorinated hyperbranched polyether copolymers for ^{19}F MRI nanotheranostics

Wanda Celentano[1,6], Giulia Neri[1], Francesco Distante [2], Min Li[3], Piergiorgio Messa[3], Cristina Chirizzi[4], Linda Chaabane[4], Floryan Decampo[5], Pierangelo Metrangolo[1], Francesca Baldelli Bombelli[1], Francesco Cellesi*[1]

[1] Dipartimento di Chimica, Materiali ed Ingegneria Chimica "G. Natta", Politecnico di Milano, Via Mancinelli 7, 20131 Milan, Italy.[2] ETH Zurich, Department of Chemistry and Applied Biosciences, Institute of Chemical and Bioengineering, Vladimir Prelog Weg 1, CH-8093 Zurich, Switzerland. [3] Renal Research Laboratory, Fondazione IRCCS Ca' Granda Ospedale Maggiore Policlinico, Via Pace 9, 20122 Milan, Italy.[4] Institute of Experimental Neurology (INSPE) and Imaging (CIS), IRCCS San Raffaele Scientific Institute, Milan, Italy, Via Olgettina 60, I-20132 Milan, Italy.[5] Solvay Specialty Polymers, Bollate, 20021 Milan, Italy. [6] Current address: Humanitas Research Hospital, Via Manzoni 56, Rozzano, 20089 Milano, Italy.

*To whom correspondence should be addressed. E-mail: francesco.cellesi@polimi.it

Dipartimento di Chimica, Materiali ed Ingegneria Chimica "G. Natta". Politecnico di Milano, Via Mancinelli 7, 20131 Milan, Italy

Phone: +39-02-23993099 Fax: +39-02-23993180

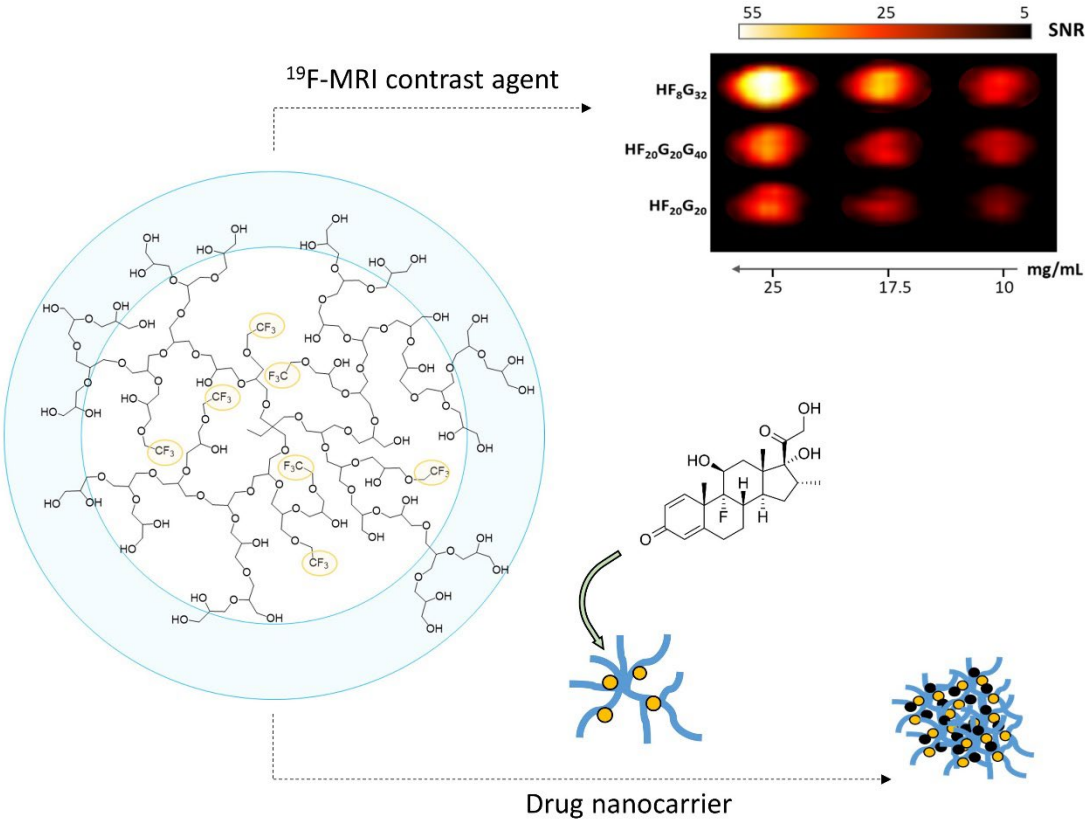

TOC. ^{19}F MRI contrast agents and drug nanocarriers based on fluorinated hyperbranched polyether copolymers.

Abstract

Fluorinated hyperbranched polyether copolymers of tuneable composition and architecture were designed and synthesized to develop drug nanocarriers as well as ^{19}F MRI contrast agents. The performance of these nanomaterials in terms of nanoparticle formation and drug (dexamethasone) loading, as well as ^{19}F-MRI detectability, was evaluated. These polymers were obtained through controlled ring opening multibranching polymerisation, and the presence of pendant fluorinated groups was obtained by copolymerisation of glycidol and the fluorinated glycidyl ether 2-[(2,2,2-Trifluoroethoxy)methyl]oxirane. By varying polymer composition and architecture during the synthesis, we controlled the key properties of the nanomaterials, including the fluorine content, drug loading, nanoparticle size, and MRI signal. The macromolecules were cytocompatible, with the ability to deliver dexamethasone on damaged kidney glomerular cells *in vitro*; therefore they hold promise as new generation ^{19}F MRI nanotheranostics.

Keywords:

Hyperbranched polyglycerol, ^{19}F-MRI, fluorinated polymer, nanocarrier, drug encapsulation, theranostics.

Introduction

Engineered polymeric nanomaterials have been extensively used in nanomedicine as nanocarriers for targeted drug delivery, as well as traceable agents for bioimaging[1]. In the field of theranostics, polymeric systems are designed to combine therapeutic and diagnostic properties[1]. In particular, hyperbranched polymers (and their well-defined analogs dendrimers) have been proposed as nanocarriers for delivery of therapeutic agents. The abundant functional groups of these complex macromolecules may undergo easy conjugation with targeting ligands and traceable groups for tissue-selective delivery and imaging purposes, respectively[2]. Moreover, hyperbranched polymers can be made amphiphilic in order to form unimolecular polymeric micelles, which are stable upon dilutions and are not affected by a critical micellar concentration[3]. This is generally advantageous for *in vivo* applications, since conventional micellar system may disassemble in the bloodstream and fail to deliver the drug at the targeted size[3, 4]. Recently, amphiphilic hyperbranched fluoropolymers have been proposed as nanoscopic ^{19}F magnetic resonance imaging (^{19}F-MRI) agents [5, 6], which are also capable of in situ drug release.

The potential of ^{19}F-MRI probes for *in vivo* tracking has recently emerged[7-10], due to the natural abundance of ^{19}F nucleus, its high sensitivity which is comparable to that of ^{1}H [11], and easy detectability due to the virtual absence of organic fluorine in living systems[12, 13].

Among different biocompatible polymers, hyperbranched polyglycerols (HPG) are a class of globular macromolecules which can be synthesized with a good control of the molar mass and functionality[14], and they have been increasingly used in a wide range of biomedical applications[15]. HPG-based macromolecules are capable of encapsulating guest (therapeutic) molecules, which may lead to the formation of unimolecular micelles in aqueous suspensions[15, 16]. Since HPGs contain a large portion of hydroxyl groups, they show hydrophilic characteristics and exhibit excellent biocompatibility and low toxicity[17, 18], which makes them

superior as drug carriers to many other hyperbranched polymers. In addition, the hydroxyl groups can be easily conjugated with different moieties, and these HPG derivatives have extended potential applications as targeted drug delivery systems[15, 19]. HPG derivatives are generally obtained from Mitsunobu and acylation reactions[20], or click reactions[21, 22]. Amphiphilic polymers can be obtained from HPG by partial functionalisation with long alkyl chains, yielding pH sensitive acetal and ketal species, thus obtaining pH-sensitive unimolecular micelles, which are able to selectively release guest molecules[23]. Similarly, reverse unimolecular micelles were obtained by partially functionalizing the HPG hydroxyl groups with palmitoyl chloride[24].

In this work, we aimed to develop novel HPG-based copolymers to serve both as ^{19}F-MRI nanoprobes and drug loaded nanocarriers, whose size and architecture can be tuned according to the different biomedical applications. Different fluorinated HPGs have been already reported to literature, even though their applications focused on non-biomedical applications (mostly as lubricants) and the functionalisation with fluorinated compounds mainly involved the outer shell of the HPG macromolecules. For example, perfluoroalkyl-functionalized hyperbranched polyglycerol were synthesized and proposed as pore forming agents in polymer microspheres (which act as supramolecular host systems)[25], and for in situ nanocoating [26]. The aggregation behaviour of perfluoro-tagged polyglycerol dendron and polyglycerol dendrimers with perfluorinated shells in water was also reported[22]. Hyperbranched fluoropolymers with a HPG core and poly(hexafluorobutyl acrylate) as hydrophobic arms, was synthesized as potential demulsifier for lubricants[27, 28]. HPGs were also used as dendritic scaffolds for the support of fluorinated alcohols, which were proposed as catalysts for the metal-free epoxidation of alkenes with hydrogen peroxide[29]. Biocompatible fluorinated (linear) polyglycerols were developed for droplet microfluidics as an alternative to PEG-based copolymer surfactants, for possible applications in cell encapsulation and *in vitro* gene expression[30] . A synthesis and

characterisation of the surface properties of fluorinated HPG, obtained by post-functionalisation with 2,2-difluoro-1,3-dimethylimidazolidine as fluorinating agent, was also reported [31].

In this work, HPG-based theranostic nanomaterials were here designed and obtained from glycidol through controlled ring opening multi branching polymerisation (ROMBP), using slow monomer addition (SMA) conditions[32-34]. The presence of pendant fluorinated groups in the hyperbranched polyether macromolecule was obtained by glycidol copolymerisation with a fluorinated glycidyl ether, such as 2-[(2,2,2-Trifluoroethoxy)methyl]oxirane, as sketched in Scheme 1. Compared with other synthetic strategies, including the post functionalisation of the HPG hydroxyl groups with fluorinated compounds, this copolymerisation allowed a better control of the grafting density, as well as the hydrophilic-lipophilic balance of the final polymer, by simply vary the molar ratio of the two monomers during the reaction. This approach offers the possibility of conjugating the inner region of the polymer chain with fluorinated groups, instead of the outer layer only.

A multistep polymerisation was also investigated in order to obtain polymer architectures characterized by an inner core containing more hydrophobic MRI traceable trifluoromethyl groups, and an outer shell with a higher density of glycerol repeating units, designed to increase the dispersibility and the colloidal stability of the polymeric nanomaterial in water. The resulting nanocarriers were characterized in terms of size distribution, drug loading, nuclear magnetic resonance properties and imaging capability, according to polymer composition and architecture. A hydrophobic fluorinated drug, i.e. dexamethasone (DEX), a synthetic steroidal anti-inflammatory drug[35, 36] was used for the scope. The cytotoxicity of these materials and their therapeutic efficacy as drug nanocarriers were finally evaluated *in vitro* on cells of the kidney filtration barrier.

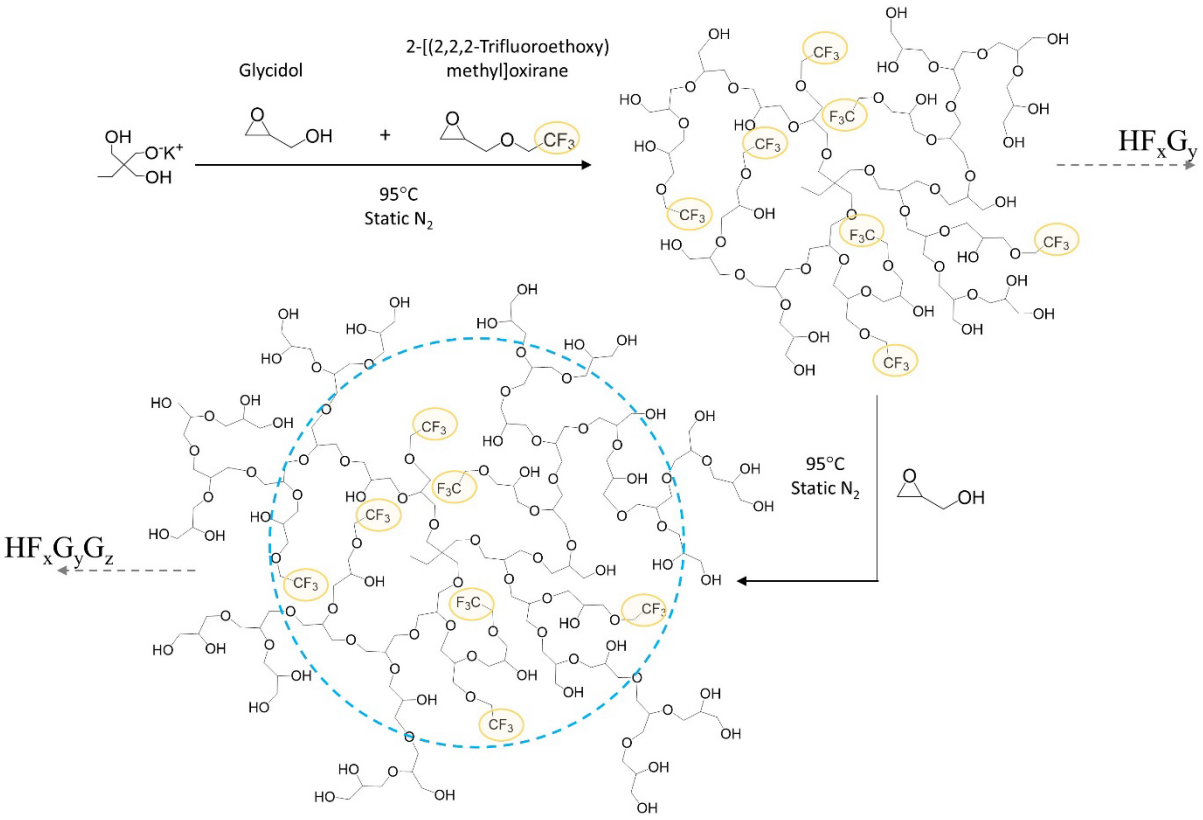

Scheme 1. Fluorinated hyperbranched polyether copolymers (HF_xG_y) were synthesized through copolymerisation of glycidol (number of glycidol repeating units y=20÷32) and 2-[(2,2,2-Trifluoroethoxy)methyl]oxirane (number of fluorinated repeating units x=8÷20). When required, a second step glycidol polymerisation was carried out to obtain the final macromolecules $HF_xG_yG_z$ (z is the number of the glycidol repeating units of the second polymerisation).

Experimental

General procedures

Reagents and solvents were purchased from Sigma-Aldrich (unless otherwise stated) and used without further purification, unless otherwise indicated. Glycidol (96%) was purified by vacuum distillation and stored in a refrigerator (2-8 °C). When anhydrous and oxygen-free conditions were required, the reactions were performed under nitrogen atmosphere. Deionized water was obtained from a Millipore Milli-Q purification unit.

^{1}H, ^{13}C, and ^{19}F Nuclear Magnetic Resonance (NMR) spectra were recorded on a Bruker AVANCE 400 MHz instrument at 298 K. Chemical shifts (δ) are reported in ppm downfield from the deuterated solvent as internal standard, coupling constants (J) in Hz.

^{19}F, T_1 and T_2 measurements were recorded at 305 K on the spectrometer operating at 400 MHz for the ^{19}F nucleus. An inversion recovery and a cpmg pulse sequences were used for the measures of T_1 and T_2, respectively.

MALDI-TOF MS analysis was performed with a Bruker LRF20 MALDI-TOF (matrix-assisted laser desorption and ionization time-of-flight) mass spectrometer, equipped with a nitrogen laser delivering 3 ns laser pulses at 337 nm. R-Cyanohydroxycinnamic acid (CHCA) was used as matrix. Samples were prepared by dissolving the polymer in methanol at a concentration of 5 mg/mL. 40 µL of this solution was added to 40 µL of a 20 g/L CHCA matrix solution in methanol and 4 µL of a cationization agent solution (0.01 M NaCl in ethanol-water 90/10). A 0.5 µL aliquot of the resulting mixture was applied to a multistage target to evaporate the methanol and create a thin matrix-analyte film. The ions were accelerated to 19 kV and measured in the reflectron mode of the spectrometer. Mainly Na-cationized ions ($M + Na^+$) were detected. Ethoxylated nonylphenols NP20 and NP100 were used for an external calibration immediately before the measurement.

GPC analysis was performed with an Agilent 1100 GPC/SEC unit, which was equipped with two PFG linear M columns (PSS) connected in series with an Agilent 1100 VWD/UV detector operated at 290 nm, a DAWN HELEOS II multi-angle laser light scattering (MALLS) detector (Wyatt Technology Europe) followed by an Optilab TrEX RI detector from Wyatt. Samples were eluted in hexafluoroisopropanol (HFIP) with 0.02 M K-TFAc at 1 mL/min at room temperature.

Dynamic Light Scattering (DLS) analyses of polymer dispersions were conducted using a Malvern Instrument Zetasizer Nano ZS instrument equipped with a 4 mW He-Ne laser operating at $\lambda = 634$ nm (backscattered angle 173°).

IR: Attenuated total reflectance FTIR (ATR-FTIR) spectra were obtained with a Thermo Scientific Nicolet iS50 FTIR spectrometer, equipped with an iS50 ATR accessory (Thermo Scientific, Madison, USA). The values were given in wavenumbers and were rounded to 1 cm^{-1} upon automatic assignment. Polymers were deposited by drop casting on the ATR probe and the solvent was evaporated before starting the measurement.

HPLC: Loading of drug was evaluated with a JASCO® High Performance Liquid Chromatography (HPLC) and the following set up: 2057 autosampler; RI-2031 refraction index detector; CO-2060 plus oven column; PU-2080 pump; MD-2018 photodiode array PDA detector; C18 column (5 μm particle size) 150 mm·4.6 mm (length × diameter).

Synthesis of 2-[(2,2,2-Trifluoroethoxy methyl]oxirane

Trifluoroethanol (10 g, 0.1 mol) and epichlorohydrin (9.2 g, 0.1 mol) were added to a cooled solution of 5 g (0.125 mol) of sodium hydroxide in 60 mL of water (2.08 M). The reactants were mixed thoroughly, and the mixture was allowed to stand at room temperature overnight. Then the organic layer was separated, washed twice with water, and dried with Na_2SO_4. The reaction product was subjected to vacuum distillation. Final yield = 11%.

^{1}H NMR (400 MHz, Methanol-*d*$_4$) δ (ppm): 4.07 – 3.88 (m, 3H, HC**H**OC**H$_2$**CF$_3$), 3.47 (m, *J* = 11.9, 6.3 Hz, 1H, HC**H**OCH$_2$CF$_3$), 3.16 (m, *J* = 6.8, 2.6 Hz, 1H, OC**H**), 2.85 – 2.73 (m, 1H, **H**CHCH), 2.61-2.59 (m, 1H, HC**H**CH). ^{13}C NMR (400 MHz, Methanol-*d*$_4$) δ (ppm): 125.58 (q, *J* = 278.1 Hz, CF$_3$), 74.16 (s, **C**H$_2$OCH$_2$CF$_3$) , 69.28 (q, *J* = 34.1 Hz, CH$_2$O**C**H$_2$CF$_3$), 51.49 (s, OCH) , 44.30 (s, O**C**H$_2$CH). ^{19}F NMR (400 MHz, MeOD) δ (ppm): -76.14 (t, *J* = 8.9 Hz). FT-IR spectrum: ν, cm^{-1}: 851, 902, 963, 1150, 1277.

Synthesis of the Hyperbranched Polyglycerol (HPG)

1,1,1-Tris(hydroxymethyl)propane (TMP) (138 mg, 1.026 mmol for HPG$_{40}$) was added to a flask under nitrogen atmosphere and it was partially deprotonated (10%) with 81 µL (1.09 mmol for HPG$_{40}$) of potassium methylate solution (25% in methanol). The mixture was stirred using a magnetic stirrer bar for 15 min at room temperature, then methanol was removed in a vacuum for 1 hour. The reaction schlenk was kept in an oil bath at 95 °C, and glycidol (2.7 mL, 40 mmol) was added dropwise over a period of 12 h using a syringe pump. After completion of monomer addition, the mixture was stirred for an additional 5 h. The reaction was monitored through ^{1}H-NMR spectra. The product was dissolved in methanol, neutralized by passing three times through a column containing cation-exchange resin (Dowex MAC-3 ion exchange resin). The polymer was then precipitated in acetone and dried under vacuum. Conversion$_{glycidol}$ > 95 %. Yield > 90%. Theoretical and measured degree of polymerisation, molar mass and dispersity are reported in Table 1.

^{1}H NMR (400 MHz, Methanol-d4), δ(ppm): 4.55 – 3.07 (m, 5H · y + 6H, OHC**H$_2$**C**H**OHC**H$_2$**O- + CH$_3$CH$_2$C(C**H$_2$**O)$_3$-), 1.68 – 1.11 (m, 2H, CH$_3$C**H$_2$**C(CH$_2$O)$_3$-), 0.88 (t, *J* = 7.5 Hz, 3H, C**H$_3$**CH$_2$C(CH$_2$O)$_3$-). ^{13}C NMR (400 MHz, Methanol-d$_4$), δ(ppm): 80.15 (d, *J* = 24.1 Hz, 1C, C$_{L13}$), 78.58 (d, *J* = 21.4 Hz, 1C, C$_D$), 72.55 (s, 2C, 2C$_{L14}$) , 71.99 – 70.49 (m, 4C, 2C$_T$+ 2C$_D$), 69.43 (d, *J* = 27.7 Hz, 2C, C$_{L13}$ + C$_{L14}$), 63.07 (d, *J* = 9.2 Hz, 1C, C$_T$), 61.44

(s, 1C, C_{L13}) . Carbons corresponding to the terminal, dendritic, linear 1,3, and linear 1,4 units are denoted by T, D, L_{13}, and L_{14}, respectively (see supporting information).

Synthesis of the fluorinated hyperbranched polyether copolymers

1,1,1-Tris(hydroxymethyl)propane (TMP) (61 mg, 0.45 mmol) was added to a flask under nitrogen atmosphere followed by 36 µL (0.49 mmol) of potassium methylate solution in methanol (25% in Methanol). The mixture was stirred using a magnetic stirrer bar for 15 minutes at room temperature. Afterwards, the excess of methanol was removed under vacuum for 1 hour. The reaction flask was kept in an oil bath at 80 °C, glycidol (0.6 mL, 9.05 mmol for $HF_{20}G_{20}$) and the fluorinated monomer (epifluorohydrin or 2-[(2,2,2-Trifluoroethoxy)methyl]oxirane) (1.1 mL, 9.05 mmol for $HF_{20}G_{20}$) were added dropwise over a period of 12 h using a syringe pump. After completion of monomers addition, the mixture was stirred for an additional 7 h.

When required, a second amount of glycidol (1.2 mL, 18.01 mmol for $HF_{20}G_{20}G_{40}$) was added dropwise over a period of 12 h using a syringe pump, at 95°C. After completion of monomer addition, the mixture was stirred for an additional 9 h. The reaction was monitored through ^{1}H-NMR spectra. The product was dissolved in methanol, neutralized by passing through a column containing cation-exchange resin (Dowex MAC-3 ion exchange resin). The polymer was then dried for 2 h under vacuum. Yield > 90%. Theoretical andmeasured degree of polymerisation, molar mass and dispersity are reported in Table 1.

^{1}H NMR (400 MHz, DMSO-d6) δ(ppm): 4.90-4.41 (m, 1H · y, **OH**$CH_2CHOHCH_2O$-), 4.04 (s, 2H · x, $OHCH_2CHOHCH_2OC\mathbf{H_2}CF_3$), 3.69-3.22 (m, *J* = 89.5, 49.5 Hz, 5H ·y + 5H · x + 6H, $OHC\mathbf{H_2}C\mathbf{H}OHC\mathbf{H_2}O$- + $OHCH_2CHOHC\mathbf{H_2}CF_3$ + $CH_3CH_2C(C\mathbf{H_2}O)_3$-), 1.28 (m, 2H, $CH_3C\mathbf{H_2}C(CH_2O)_3$-), 0.79 (s, 3H, $C\mathbf{H_3}CH_2C(CH_2O)_3$-).

Polymerisation kinetics

Homopolymerisation of glycidol (GLY) (target DP=40), fluorinated glycidyl ether (FGE) (target DP=40), and copolymerisation of GLY and FGE (feed molar ratio 1:1, target DP=40), were carried out according to the SMA method as described above. 30 μL of reaction mixture were collected at different times (15 min, 30 min, and every hour up to 8 hours), cooled at room temperature before addition 0.5 mL of deuterated solvent (Methanol-d4 for GLY and FGE polymerisation, DMSO-d6 for GLY-FGE copolymerisation), and analysed by ^{1}H NMR. Due to the small reaction volumes available at 15 and 30 min, two additional reactions were carried out in parallel and stopped at these time points for analysis.

In Methanol-d4, the resonance peak at 0.88 ppm (corresponding to the methoxy protons of TMP) was set as a reference. For GLY and FGE polymerisation, the degree of polymerisation (DP) was evaluated by quantifying the amount of residual monomer in the reacting mixture, by integrating the peak at 2.63 ppm, which correspond to one proton of the monomeric oxirane (1H, C**H**$_2$CH). For GLY-FGE copolymerisation, the average number of GLY and FGE repeating units (n_{OH} and n_F , respectively) of the growing polymer chains were calculated by integrating the peaks which correspond to the protons of the residual monomers in DMSO-d6, i.e. at 2.58 ppm (FGE, 1H, C**H**$_2$CH), 2.67 ppm (GLY, 1H, C**H**$_2$CH), 2.75 ppm (FGE, 1H, CH$_2$C**H**), 2.98 ppm (FGE, 1H, CH$_2$C**H**). The resonance peak at 0.79 ppm (corresponding to the methoxy protons of TMP in DMSO-d6) was set as a reference.

Drug loading

10 mg of polymer were dissolved in a flask with 1 mL of deionized water and the solution was stirred for 15 minutes. A stock solution of DEX in Acetone (1 mg/mL) was prepared in a vial and stirred for 15 minutes. 1 mL of this solution was added dropwise to the polymer solution under stirring. Evaporation of acetone was performed under reduced pressure at 40°C. Polymer

nanoparticles without DEX were obtained by dispersing the polymer under the same conditions but without addition of the drug. The obtained mixture was diluted in 2 mL of deionized water and centrifuged at r.t, 10000 rpm for 15 minutes. The final suspension was then placed in a cuvette to perform the DLS test. The suspension was transferred into a vial and lyophilized overnight. The lyophilized polymer was dissolved in 1 mL of Acetonitrile:H_2O (1:1), then diluted 1:10 or 1:100 to prepare 1mL of polymer solution in Acetonitrile:H_2O (1:1), and the DEX content was determined by HPLC analysis. Each sample was injected (10 µL) in a C18 reversed-phase chromatography column (particle size 5 µm, length 150 mm, Restek Corporation U.S.) at 35°C with a flow rate of 1 mL/min in a solution of Acetonitrile: H_2O (1:1). The DEX peak was detected after 3.2 min approximately; the UV detection wavelength was set at 254 nm. Calibration curve was previously obtained with different DEX concentration (1-0.001 mg/mL). The Drug Loading (DL%) and Encapsulation Efficiency (EE%) values associated to each polymer were calculated according to the following equations:

$$DL\% = \frac{Drug\ Loaded\ [mg]}{Drug\ Loaded\ [mg] + Polymer\ mass\ [mg]}\%; \qquad EE\% = \frac{Drug\ Loaded\ [mg]}{Drug\ Feeded\ [mg]}\%$$

Drug release

Release studies were conducted via HPLC by dialyzing 1 mL of DEX-loaded NPs suspension (prepared from 5 mg of DEX and 50 mg of polymer) in 200 mL of PBS 10 mM at 37 °C (regenerated cellulose dialysis membrane, 3500 Da cut-off). At selected times, small aliquots (200 µL) were withdrawn and replaced with an equal volume of PBS. Each sample was analysed by HPLC to determine the concentration of DEX. The HPLC system (Jasco) was equipped with a Restek C18 column and a photodiode array PDA detector. The detector wavelength was set at 254 nm, and the mobile phase was composed of water and acetonitrile (50/50 v/v) in isocratic condition at a flow rate of 1 mL/min at 35 °C.

Magnetic Resonance Imaging

Polymer samples were prepared by dissolving the fluorinated polymers in D_2O at different concentrations (25.0 mg/mL, 17.5 mg/mL, 10 mg/mL). Magnetic Resonance Imaging (MRI) was performed using a 7 Tesla scanner (Bruker-Biospin) with a double tuned ^{1}H-^{19}F radiofrequency coil for excitation and reception. MRI data were acquired using a 3D-Fast-spin echo sequence with the resonance frequency fixed on ^{19}F (282.6 MHz) with a field of view of 45x30x28 and a matrix of 64x32x8. The repetition and echo times were fixed to optimized values (3000 and 56 ms, respectively) for high sensitivity. Due to the long T_2 relaxation time of ^{19}F-polymers, a large rare factor (14 echoes) was used to reduce the acquisition time (40 min with 100 signal averages). The relaxation times T_1 and T_2 were measured using a 2D-spin echo with multiple repetitions times (0.25 to 5.5 sec) and echo times (24 to 224 ms). The relaxation times were calculated using the fitting tools of the scanner program (Paravision 6, Bruker-Biospin). The signal to noise ratio (SNR) was calculated as the ratio of the mean signal intensity of each sample divided by the standard deviation of the noise from the background. An emulsion of a superfluorinated compound (PERFECTA[12]) were used at fixed concentrations (0.4 and 0.6 $x10^{20}$ ^{19}F atoms/mL) as reference.

LDH Cytotoxicity

NPs cytotoxicity was measured using LDH-Cytotoxicity Colorimetric Assay Kit (BioVision Incorporated). Briefly 8000 per well of conditionally immortalized human podocytes (HCiPodo) or conditionally immortalized human glomerular endothelial cells (HCiGEnC) (both from University of Bristol, Bristol, UK) were plated on a 96-well plate and cultured at 37°C respectively in RPMI-1640 with 10% FCS, 5 μg/mL transferrin, 5 ng/mL sodium selenite, 0.12 U/mL insulin, 100 U/mL penicillin, 100 mg/mL streptomycin or with EGM2-MV medium containing foetal calf serum (5%) and growth factors as supplied (Lonza,

Walkersville, MD, USA) for 3-4 days. Then, the culture medium was replaced by medium containing different concentration of NPs (0.01-2mg/mL) which was incubated with cells for 24 hours. For positive control (high control), 10 µL of cell Lysis solution was added and incubated for 24 hours, while the low control was referred to cells incubated only with standard medium. At the end of incubation, the plate was gently shacked for some minutes and centrifuged at 600 x g for 10 min. 10 µL of culture medium from each well was transferred into a new optically clear 96-well plate, and 100 µL of LDH Reaction Mix was added to each well and incubated at room temperature for 30 min. The absorbance of all controls and samples was measured with 450 nm filter using SAFAS Spectrophotometry (Monaco). The cytotoxicity was calculated using the equation: Normalised Cytotoxicity = (Test sample-Low control)/(High control-Low control); Low control : normal cells; High control : cells treated with lysis buffer.

Fluorescence Microscopy Examination

HciPodo and HCiGEnC were cultured on coverslips and fixed with 4% of paraformaldehyde at room temperature for 10 min. After washing, cells were permeabilized with 0.3% of Triton in PBS for 5 min and incubated with 1% of bovine serum albumin in PBS at room temperature for 30 min. Phalloidin-FITC (Sigma-Aldrich) at 1:100 dilution together with DAPI at 1:1000 dilution (Sigma-Aldrich) was added, and the cells were incubated for 1 h. After 3 times washing with PBS, the cells were mounted with Fluorsave aqueous mounting medium (Merck, Milano, Italy). Images were acquired using a Zeiss AxioObserver microscope equipped with a highresolution digital videocamera (AxioCam, Zeiss) and an Apotome system for structured illumination, and recorded by the AxioVision software, version 4.8.

DEX Release on Podocytes

HciPodo cells were plated on a 35 mm Petri dish containing four cell culture coverslips and cultured at 37 °C for 3−4 days. Afterwards, cells were incubated with 0.8 μM Adriamycin (ADR, Sigma-Aldrich) in cell culture medium for 24 h. After 24h incubation, ADR was replaced by fresh medium (as the control group) or medium with a nanoparticle suspension (HF_8G_{32}) containing DEX (10 μM), and incubated for another 24 ÷ 48 h. Cells were finally washed thrice with PBS and characterized by fluorescence microscopy as described above.

Results and discussion

Hyperbranched polyglycerols (HPG_s) were synthesized through a Ring Opening MultiBrancing Polymerisation (ROMBP) of glycidol[32, 33, 37], initiated by partially deprotonated trimethylolpropane (TMP). The Fluorinated Hyperbranched polyether copolymers (HF_xG_y) were synthesized through copolymerisation of glycidol (number of glycidol repeating units y=20÷32) and the fluorinated glycidyl ether (number of fluorinated repeating units x=8÷20) (Scheme 1). This fluorinated co-monomer (e.g. 2-[(2,2,2-Trifluoroethoxy)methyl]oxirane), was previously synthesized by treating trifluoroethanol with epichlorohydrin in presence of an excess of sodium hydroxide in water, and the product was isolated from the organic phase by vacuum distillation[38-40](see supporting information). When required, the hydrophilicity of the macromolecules was enhanced by a second-step polymerisation, which was easily carried out by subsequent addition of glycidol to the active alkoxide chain ends of the copolymers (Scheme 1), thus obtaining the final macromolecules $HF_xG_yG_z$ (z is the number of the glycidol repeating units of the second polymerisation). All the polymerisations were carried out in bulk (80÷95 °C) and monomers were slowly added (dropwise, by using a syringe pump[32], according to the SMA method[32-34]) over a period of 12 h, and the final mixture was allowed to react under stirring for additional 5-7 h. High conversions (> 95%) were obtained for all the polymerisations, according to the values calculated by ^{1}H-NMR spectra in DMSO-d_6 (Figure

1A). The signals of the CH_x backbone was represented by the peaks between 3.1 and 3.9 ppm and the peak at 4.04 ppm corresponded to the CH_2 next to the trifluoromethyl group. The hydroxyl protons resonated between 4.3 and 5.0 ppm. The signals of the methyl and the methylene group of TMP at 0.79 and 1.28 ppm, respectively, confirmed the incorporation of the initiator in the final polymer. ^{19}F-NMR spectrum in DMSO-d_6 also confirmed the presence of the fluorinated repeating units with a broad peak at -73.3 ppm; the equivalents of fluorinated groups conjugated with the polymer were quantified by adding 2,2,2-Trifluoroethanol (signal at -75.5 ppm) as reference(Figure 1B).

A

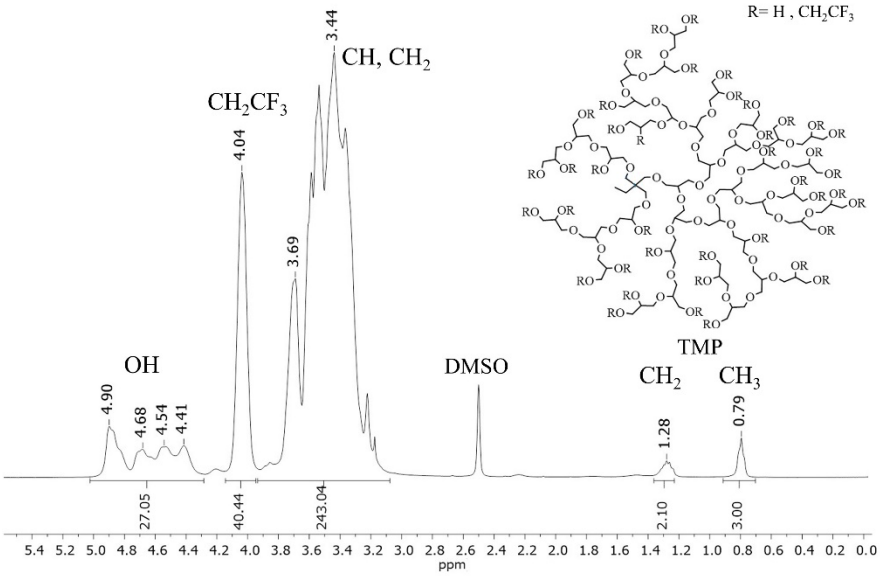

B

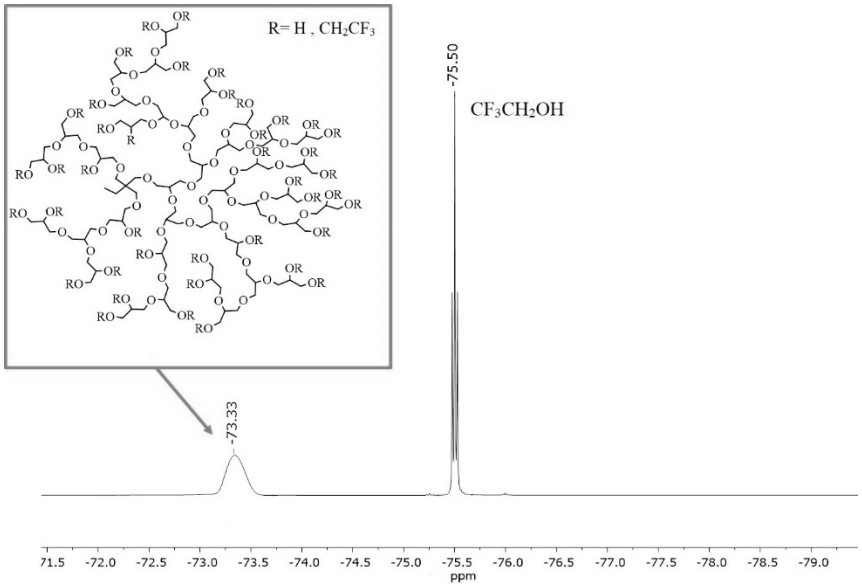

Figure 1. A) ^{1}H-NMR (DMSO-d_6) of $HF_{20}G_{20}$. B) ^{19}F-NMR spectrum of $HF_{20}G_{20}$ (DMSO-d_6) with 2,2,2-Trifluoroethanol as reference.

In order to evaluate the composition of the growing copolymers in the course of the reaction, kinetic studies were carried out by monitoring the polymerisation at fixed time points and

analysing the ratios of polymer repeating units, unreacted monomers and initiator by ^{1}H NMR[34, 41] (see supporting information).

Since the characterisation of total monomer conversion is not feasible for polymerisations under SMA conditions[34], the average degree of polymerisation (DP) was calculated as function of the reaction time (Figure 2A). Homopolymerisation of the fluorinated glycidyl ether (FGE) showed a linear chain growth as seen for glycidol (GLY), but at slower rate (K_{GLY}=0.05 r.u./min, K_{FGE}=0.03 r.u./min). The different reactivity of the two monomers did not alter the chain composition when the two monomers were copolymerised in a 1:1 feed ratio (Figure 2B). The average number of GLY and FGE repeating units (n_{OH} and n_F, respectively) of the growing polymer chains increased linearly with time, and the chain fraction of FGE repeating units (f_F) remained almost constant (f_F ~ 48.5%) during the reaction.

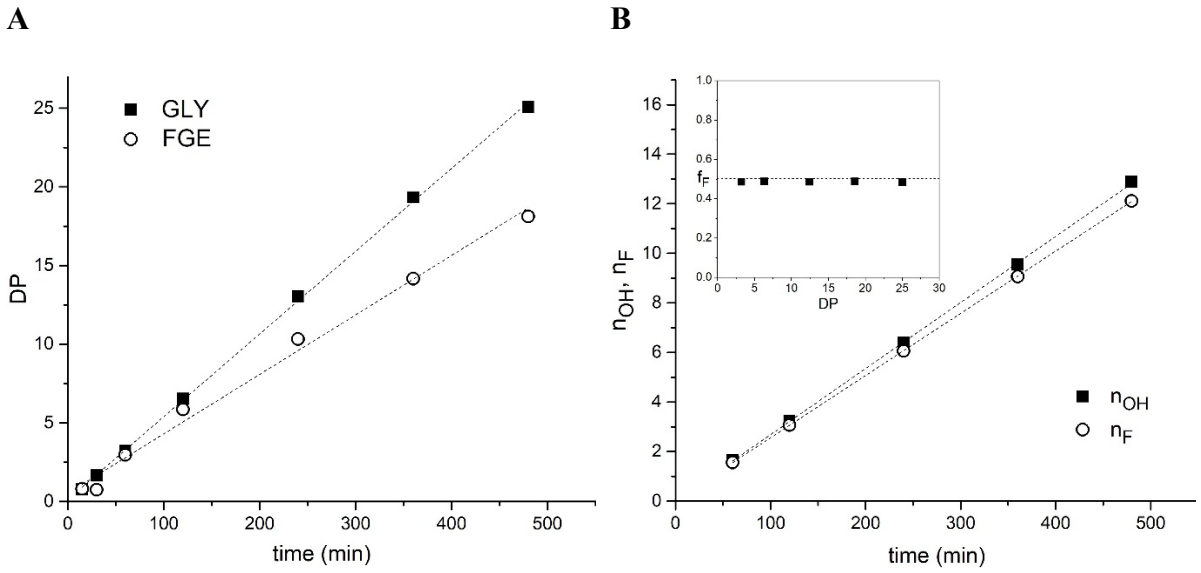

Figure 2. A) Degree of polymerisation of glycidol (GLY) and fluorinated glycidyl ether (FGE) over reaction time under SMA conditions. B) Copolymerisation kinetics of GLY-FGE mixture (molar ratio 20:20). n_{OH} and n_F are the average number of GLY and FGE repeating units of the growing polymer chains, respectively. Inset: chain fraction of FGE repeating units (f_F) as function of the total average degree of polymerisation (DP).

MALDI-TOF mass spectrometry was also used to confirm that the fluorinated monomer was incorporated as repeating unit into the hyperbranched macromolecules (Figure 3). In the MALDI-TOF spectrum of non-fluorinated hyberbranched polyglycerol, the mass differences between the peaks precisely representedthe molar mass of glycidol (M=74 Da). A subdistribution of peaks shifted by 14-16 mass units was also shown, which was most likely due to the presence of linear or (macro)-cyclic polyglycerol macromolecules which lack the TMP core, in agreement with previous work by Frey and coworkers[33]. The presence of this sub-population may have an effect on the final physicochemical properties of the nanomaterials, particularly in terms of colloidal properties and drug delivery, although its contribution is difficult to quantify. The spectrum of fluorinated polyether copolymer confirmed the random copolymerisation of the fluorinated monomer, as the mass differences between the peaks precisely representedthe molar mass of trifluoroethoxy methyl oxirane (M=156 Da) and that of glycidol, in a random pattern.

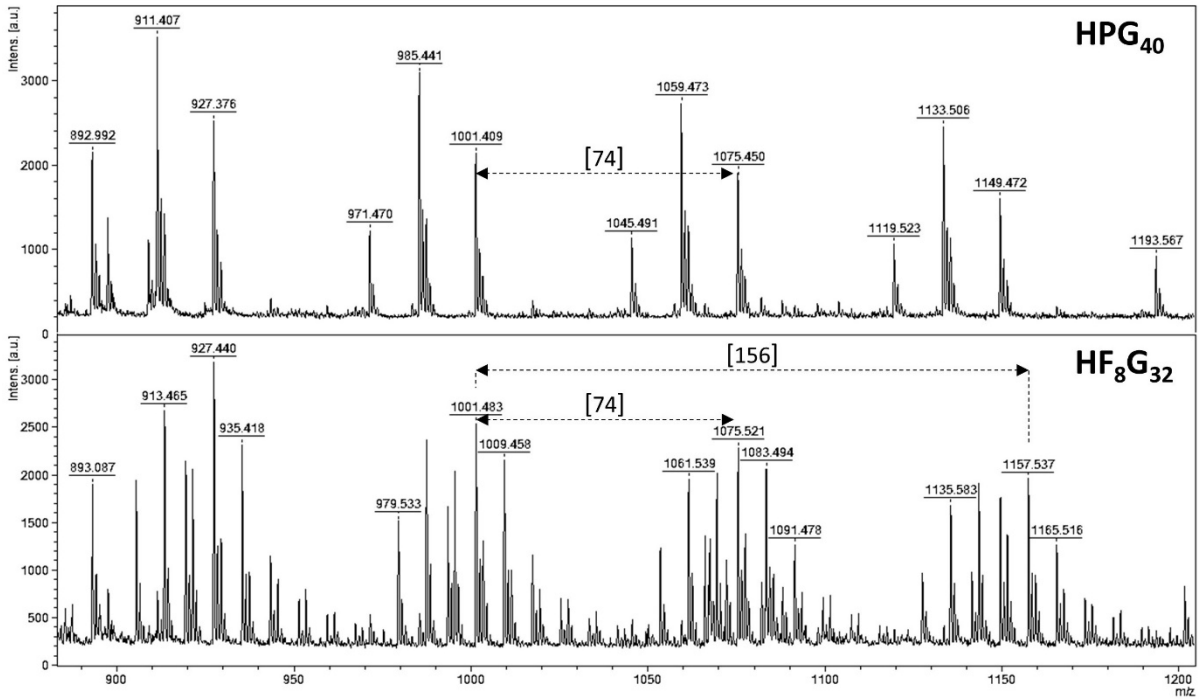

Figure 3. MALDI-TOF mass spectra of hyperbranched polyglycerol HPG_{40} (top) and the fluorinated macromolecule HF_8G_{32} (bottom).

A summary of the characteristics of the synthesized macromolecules are reported in Table 1, including the degree of polymerisation of the glycidol (DP_{OH}) and the fluorinated repeating unit (DP_F) (both theoretical and as calculated by NMR analysis), the average molar mass and the dispersity (Đ) calculated by GPC analysis. Taking into account the intrinsic limitation of GPC to determine the exact number- and weight- average molar mass of hyperbranched polyglycerols (which is related to the interaction of the multifunctional polymer with the column, the correct calibration, the detector and the choice of solvent), the Đ values were obtained in the range of 1.2÷1.6, in agreement with previous studies on ROMBP of glycidol[32, 33, 37].

Table 1. Summary of the fluorinated and non-fluorinated hyperbranched polyethers with characteristics and properties.

Name	**$DP_{OH,Th}$**	**$DP_{F,Th}$**	**$M_{n,Th}$ (Da)**	**$DP_{OH,NMR}$**	**$DP_{F,NMR}$**	**M_{nNMR} (Da)**	**M_{nGPC} (Da)**	**M_{wGPC} (Da)**	**Đ**
HPG_{40}	40	0	3000	48	0	3719	2890	3520	1.22
HPG_{80}	80	0	6000	100	0	7555	2450	3910	1.60
HF_8G_{32}	32	8	3753	32	7.8	3719	3100	4480	1.45
$HF_{20}G_{20}$	20	20	4738	27	20	5288	2710	3920	1.45
$HF_{20}G_{20}G_{40}$	60	20	7580	61	19	7619	3480	5100	1.47
$HF_{20}G_0G_{40}$	40	20	7990	27	33	7286	3230	3860	1.20

Nanoparticle formation and DLS

Nanoparticle formation was carried out by dispersing the polymer in water, while the self-assembly of the colloids in presence of the hydrophobic drug was obtained by dropwise addition of a DEX solution in acetone, followed by removal of the volatile organic solvent under reduced pressure[35, 42]. A centrifugation step was also carried out to remove the unloaded drug precipitate, before characterisation of the size distribution of the nanoparticles by DLS, and determination of the drug loading (DL%) and the encapsulation efficiency (EE%) by HPLC. Results are summarized in Table 2.

Table 2. Drug loading (DL) and Encapsulation efficiency (EE) determined by HPLC after DEX loading at 25°C. Average size and size polydispersity index measured by DLS with and without DEX encapsulation. Centrifugation yield is referred to % polymer mass recovered after centrifugation. (*scattering intensity too low for a reliable determination of d_h)

Polymer	Centrif. yield (%)	DL% (±SD)	EE% (±SD)	d_h w/o drug loading [nm]	PdI	d_h after drug loading [nm]	PdI
HPG_{40}	95	0.1±0.1	1.0±1.0	n.d*	n.d*	165	0.1
HF_8G_{32}	94	4.2±0.1	39.7±1.1	157	0.5	164	0.3
$HF_{20}G_{20}$	90	4.4±0.1	39.6±1.0	886	1.0	211	0.2
HPG_{80}	98	0.2±0.2	2.0±2.0	3	0.1	189	0.1
$HF_{20}G_{20}G_{40}$	91	2.9±0.1	26.7±0.1	365	0.2	212	0.2

The presence of the hydrophobic fluorinated groups in HF_8G_{32}, $HF_{20}G_{20}$ and $HF_{20}G_{20}G_{40}$ enhanced the DL% and EE% when compared with the non-fluorinated polyglycerols at the same degree of polymerisation. The amount of drug loaded was dependent on the ratio between the fluorinated and non-fluorinated repeating units, as well as the molar mass. The highest drug loading (4.4%) was obtained with $HF_{20}G_{20}$, which is the polymer with the highest $–CF_3$ content. Similar DL% was obtained with HF_8G_{32}, which presented a lower $–CF_3$ content than $HF_{20}G_{20}$, but also a lower molar mass, which may have a positive effect on the self-assembly mechanism of this drug-polymer system.The macromolecule $HF_{20}G_0G_{40}$, which was obtained by a first homopolymerisation of trifluoroethoxy methyl oxirane followed by a second glycidol polymerisation, was unable to form stable colloidal particles in water (DLS autocorrelation function shown in the supporting information, Figure S9). In this case, the steric repulsion of

the hydrophilic shell was not strong enough to avoid the aggregation of the linear fluorinated blocks and prevent macroscopic phase separation, therefore this polymer was not investigated further in this study.

The size distribution of the nanoparticles wascharacterised by DLS before and after drug loading (Table 2 and Figure 4). Due to the hydrophobicity of the fluorinated groups, polymers in water self-assembled in relatively large colloids, and showed broad size distribution curves (often multimodal) with high polydispersity index.

In presence of DEX, the self-assembly provided a much narrower size distributions with much lower Z-average diameter, suggesting that the hydrophobic drug may ameliorate the phase separation between the (inner) hydrophobic and the (outer) hydrophilic domains, thus enhancing the colloidal stability. After centrifugation, the percent of polymeric mass recovered (as weighted after freeze dying) was above 90% (Table 2) and this may indicate that the difference of particle size before and after drug loading was not due to the removal of larger particles, but rather to a general improvement of the self-assembly with the drug.

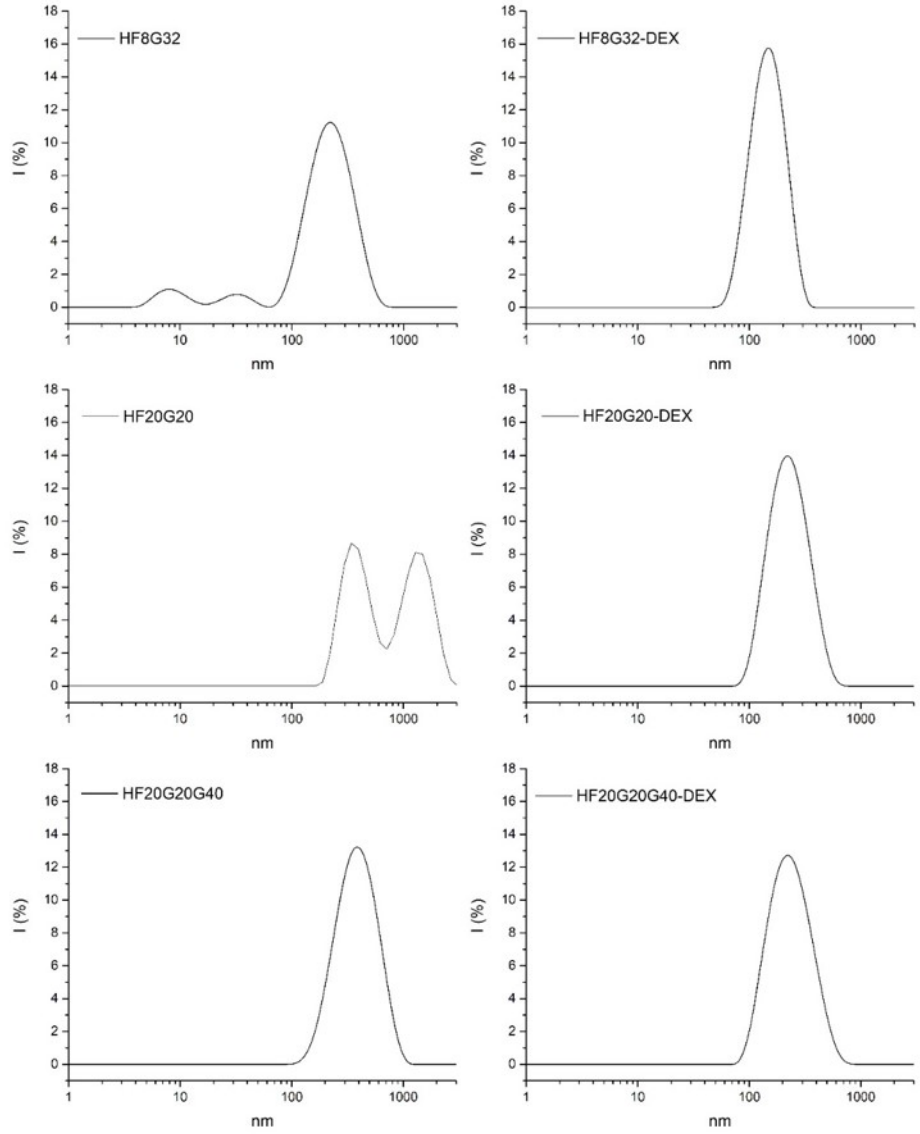

Figure 4. DLS Intensity size distributions of fluorinated macromolecules before (left) and after (right) DEX nanoencapsulation (H_2O, 25°C, 10 mg/mL).

As expected, the final particle size was dependent on the polymer molar mass as well as the -CF_3 content. At low DP_F of fluorinated repeating units, the polymer (HF_8G_{32}) after drug loading showed a Z-average size comparable with that of pure polyglycerol at similar molar mass (HPG_{40}). As the DP_F increased ($HF_{20}G_{20}$), the average size increased of ~50 nm. The additional step of glycidol copolymerisation in $HF_{20}G_{20}G_{40}$ did not increased the particle size substantially. This result suggested that the higher hydrophilicity of the macromolecule was

counterbalanced by the increase of the molar mass. On the other hand, the hydrodynamic diameter of DEX-loaded $HF_{20}G_{20}G_{40}$ was slightly higher (< 20 nm) than that of pure polyglycerol at similar molar mass (HPG_{80}), and this may be ascribed to the effect of the trifluoromethyl group in forming larger colloidal aggregates.

^{19}F MR Imaging

The ^{19}F imaging capability of these hyperbranched polymers was further evaluated on a 7 Tesla scanner. All polymers exhibited a clear ^{19}F MR imaging ability, with a positive correlation between the polymer-fluorine concentration and the signal-to-noise ratio (SNR) (Figure 5, Table 3). Polymers with lower amount of fluorinated repeating units showed an unexpected higher SNR than that of polymers with increased fluorine content (Figure 5). This result may indicate that a relatively low –CF3 content may limit the strong dipolar interactions between the highly hydrophobic fluorinated groups[43, 44], with the advantage of enhancing the mobility of the ^{19}F nuclei[45, 46].

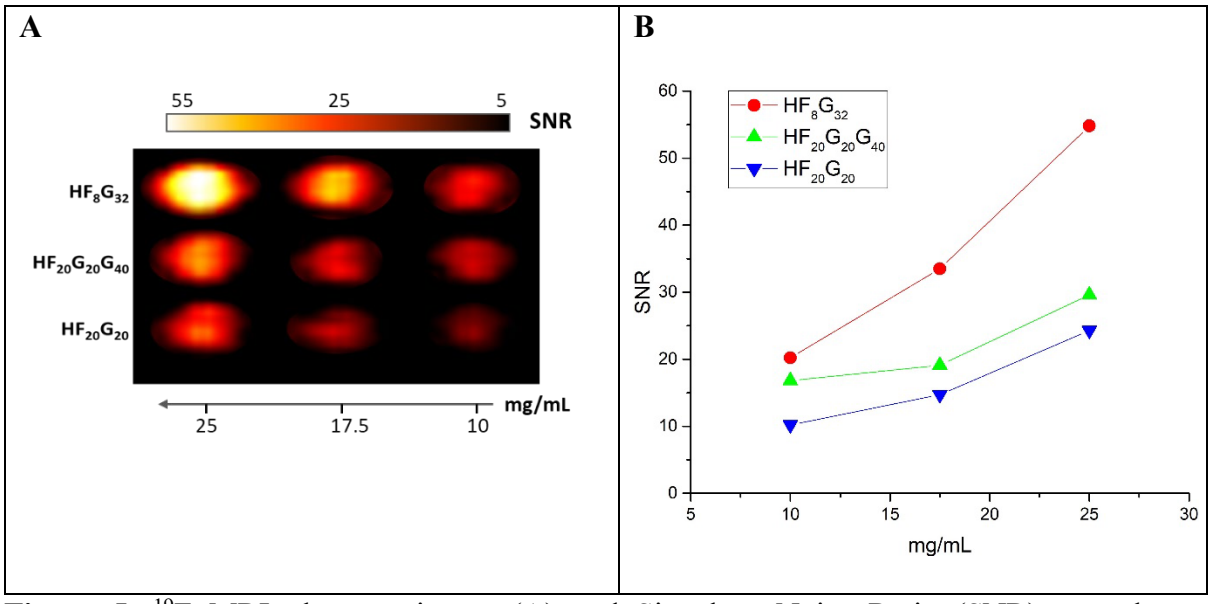

Figure 5. ^{19}F MRI phantom image (A) and Signal to Noise Ratio (SNR) vs polymer concentration (B) of hyperbranced fluorinated polyethers (HF_8G_{32}, $HF_{20}G_{20}$, $HF_{20}G_{20}G_{40}$).

The highest SNR signal was obtained with the polymer HF_8G_{32}, which not only had the lowest fluorine content, but also the smallest particle size, and this may confirm the key role of this physical parameter in ^{19}F-MRI polymeric contrast agents[44]. By comparing the two polymers with similar particle size ($HF_{20}G_{20}$ and $HF_{20}G_{20}G_{40}$), it was noticed that the one with lower fluorine content showed brighter images, thus confirming that an excess of hydrophilic (hydroxyl) groups may ameliorate the mobility of the fluorinated domains [46]. No significant variation of the SNR was recorded when DEX was encapsulated in the polymer nanoparticles (Figure S10, supporting information), in accordance to the negligible contribution of the F atom of the DEX molecules at a drug loading (DL) < 5%.

Due to their relatively long T_1 (Table 3), these nanomaterials may require long image acquisition times to obtain a sufficiently high SNR *in vivo* [43, 47], therefore they may not be convenient as blood pool contrast agents[5]. However, they may be suitable for ^{19}F MRI theranostics when used as nanocarriers for cell tracking or passive-active targeting purposes, as they can induce local enhancement of fluorine concentration in cells and tissues[5, 48].

Table 3. Dependence of ^{19}F MRI signal to noise ratio (SNR) on polymer concentration (mg/mL), ^{19}F atom concentration, T_1 and T_2 relaxation times of hyperbranched fluorinated polyether dispersions.

Molecule	T_1(ms)	T_2(ms)	Conc. (mg/mL)	(x10^{20}) ^{19}F/mL	SNR
HF_8G_{32}	1294	504	25.0 17.5 10.0	0.95 0.66 0.38	54.8 33.5 20.2
$HF_{20}G_{20}$	366	290	25.0 17.5 10.0	1.7 1.2 0.68	24.3 14.7 10.2
$HF_{20}G_{20}G_{40}$	666	229	25.0 17.5 10.0	1.13 0.79 0.45	29.6 19.1 16.8

In vitro cytotoxicity

The fluorinated polyether copolymers were assessed in terms of cytotoxicity *in vitro*. Immortalized human glomerular endothelial cells (HCiGEnC) and immortalized human podocytes (HCiPodo) were selected for the tests, as cells of the glomerular filtration barrier in kidneys would constantly interact with the nanomaterials *in vivo* [35, 49]. Cells were cultured at 37 °C with a medium containing different concentration of polymers (0.01÷2 mg/mL) for 24 h. Lactate Dehydrogenase (LDH) colorimetric assay was used to quantify the amount of the cytosolic LDH enzyme released by damaged cells, since it was proven to be an efficient indicator of cytotoxicity for kidney glomerular cells[35, 36]. All polymeric nanocarriers (with or without drug loading) showed negligible cytotoxicity up to a concentration of 1 mg/mL (Figure 6), which confirmed the high biocompatibility of these polymeric nanomaterials.

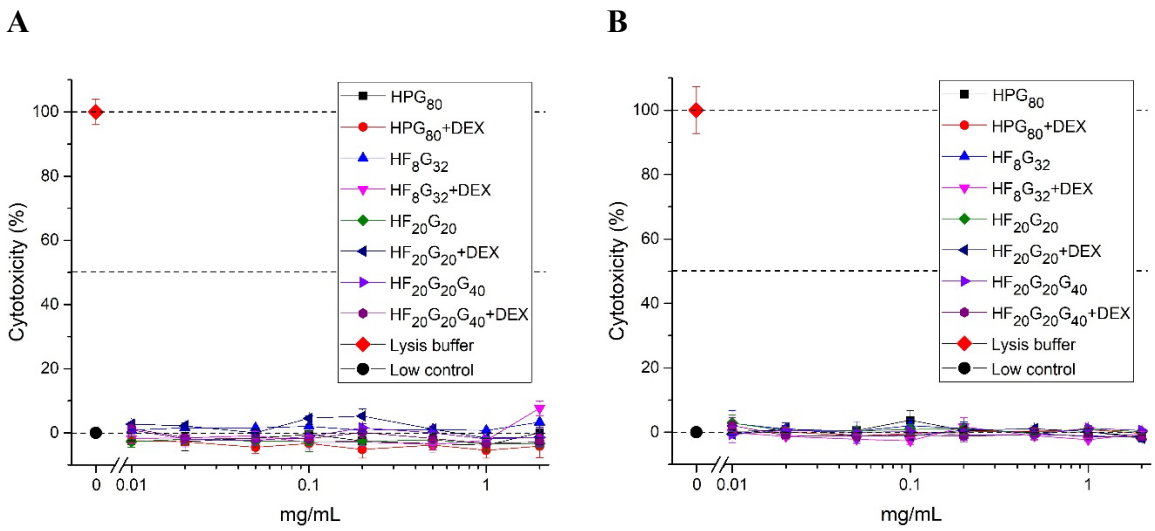

Figure 6. LDH assay on HCiGEnC (A) and HCiPodo cells (B) incubated with polymers (HPG_{80}, HF_8G_{32}, $HF_{20}G_{20}$, $HF_{20}G_{20}G_{40}$, with and without loaded DEX) for 24 h, at concentration from 0.01 to 2 mg/mL. Y-axis: Normalised Cytotoxicity (%) = (Test sample-Low control) / (High control-Low control) x 100; Low control: normal cells with no polymer added; High control: cells treated with lysis buffer, with no polymer added.

DEX Release on damaged podocytes

Finally, we investigated the therapeutic effect of DEX release form these polymeric nanomaterials *in vitro*. It has been reported that alteration of the cytoskeleton morphology (F-actin orientation) of podocytes is a good indicator of pathological condition in chronic kidney diseases[50], and that the effect of DEX release on these cells can be assessed by evaluating their F-actin orientation before and after the treatment[35, 36]. Cytoskeleton damage was induced by treating podocytes with Adriamycin (ADR) for 24 h, as confirmed by the reduced density and irregular distribution of the actin fibres (stained by phalloidin), together with shortening or disappearance of protrusions (Figure 7B). A suspension of DEX-loaded HF_8G_{32} nanoparticles was selected for the test, since this formulation achieved the best combination of high drug loading and small particle size, together with the highest SNR signal in MRI. These nanoparticles guaranteed an ~85% DEX release in 48 h (Figure 7A). After 48 h of incubation

of the cell culture with the nanoparticles, podocytes displayed a more regular distribution of F-actin along the whole cell body and processes, thus recovering their healthy morphology (Figure 7B-F). Damaged cells which were untreated, treated with unloaded nanoparticles, or treated with DEX-loaded HF_8G_{32} for only 24h, did not show evidence of morphological response. These results demonstrated that DEX bioactivity was retained during nanoencapsulation and release.

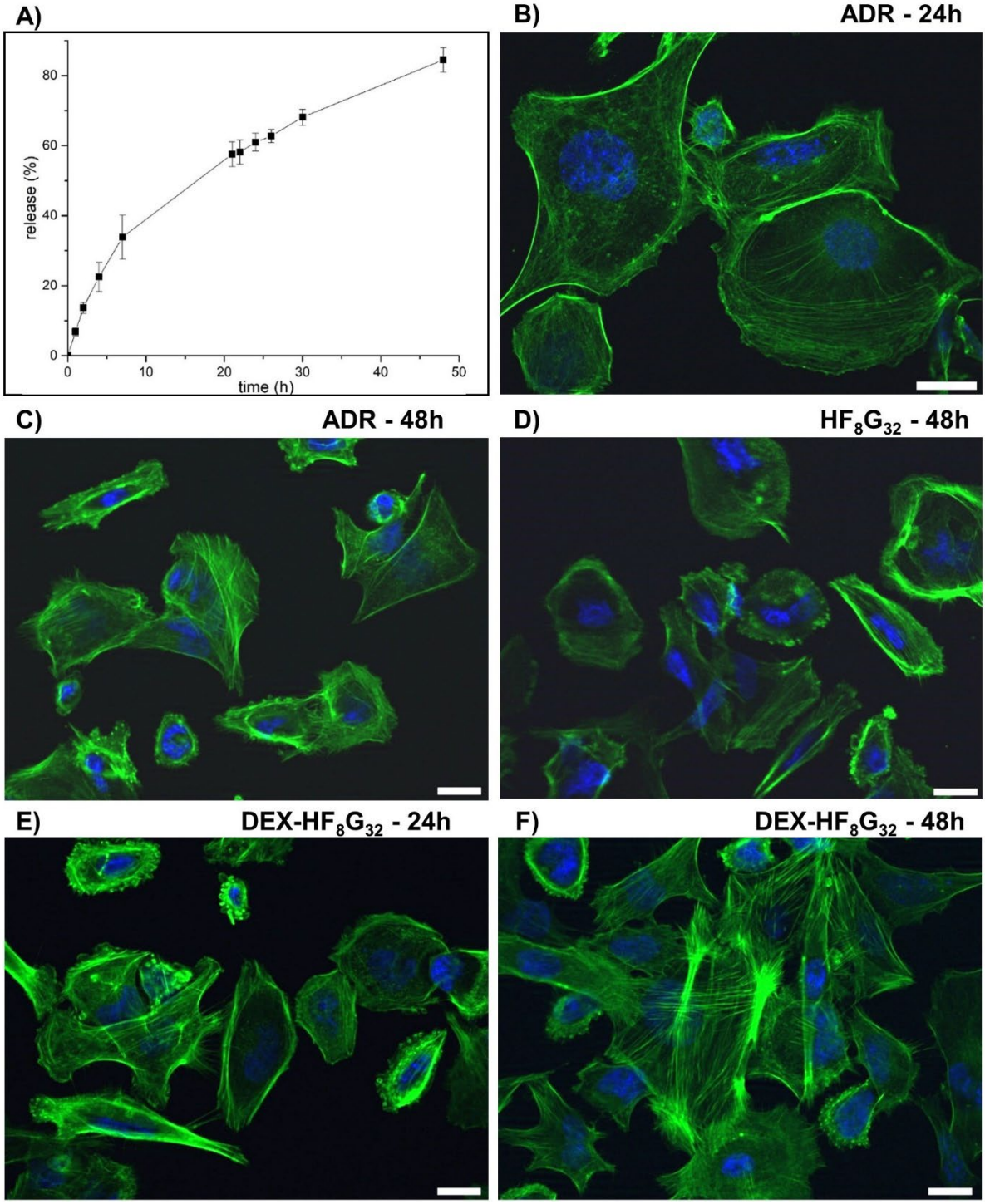

Figure 7. A) DEX release from HF_8G_{32} polymeric nanoparticles in water at 37 °C (error bars indicate± SD from experiments run in triplicate). HCiPodo cells (stained by green phalloidin and DAPI, scale bar 20 μm) damaged by ADR and incubated as follows: in absence of polymer nanoparticles for 24 h (B) and 48 h (C), with unloaded HF_8G_{32} for 48 h (D), with DEX-loaded HF_8G_{32} (DEX concentration 10 μM) for 24 h (E) and 48 h (F).

Conclusions

A series of fluorinated hyperbranched polyether copolymers was successfully synthesized and studied for the design of ^{19}F MRI nanotheranostics. The aim of the study was to evaluate the performance of these nanomaterials in terms of nanoparticle formation and drug (DEX) loading, as well as ^{19}F-MRI detectability. By varying the polymer composition and architecture during the synthesis, the properties of these macromolecules were tuned in terms of fluorine content, drug loading, particle size, MRI signal.

NMR, MALDI-TOF and GPC analysis confirmed the efficient copolymerisation of glycidol and trifluoroethoxy methyl oxirane, through controlled ROMBP under slow monomer addition conditions. The self-assembly of the copolymers with DEX in water provided nanoparticle suspensions with a relatively narrow size distribution, and a drug loading which was dependent on the molar mass and the ratio between the fluorinated and non-fluorinated repeating units.

The ^{19}F MRI performance suggested that these nanocarriers may be used for cell tracking or passive-active targeting purposes, by inducing local enhancement of fluorine concentration in the biological environment. The nanomaterials also showed negligible cytotoxicity and clear capability to repair damaged kidney glomerular cells *in vitro*.

Conflicts of interest

There are no conflicts to declare.

Author Contributions

The manuscript was written through contributions of all authors. W.C. designed and performed polymer and nanomaterial synthesis, physicochemical characterisation, and data analysis. G.N. and F.D. performed polymer characterisation. M.L. and P.M designed and performed the biological tests. C.C. and L.C designed and performed MRI tests. F.D, P.M and F.F designed experiments and supervised the research, F.C. designed experiments, supervised the research and was a major contributor in writing the manuscript. All authors read and approved the final manuscript.

Acknowledgements

The financial support from Solvay Specialty Polymers is gratefully acknowledged.

The authors thank Prof. Giuseppe Storti (Department of Chemistry, Materials and Chemical Engineering, Politecnico di Milano, Italy), and Dr Stéphane Goyard (Laboratoire d'Analyse, Solvay, France) for their assistance with GPC tests and MALDI-TOF analysis, respectively.

References

1. T. Krasia-Christoforou and T. K. Georgiou, *Journal of Materials Chemistry B*, 2013, **1**, 3002-3025.
2. Y. Zheng, S. Li, Z. Weng and C. Gao, *Chemical Society Reviews*, 2015, **44**, 4091-4130.
3. S. Ordanini and F. Cellesi, *Pharmaceutics*, 2018, **10**.
4. A. V. Fuchs, A. P. Bapat, G. J. Cowin and K. J. Thurecht, *Polymer Chemistry*, 2017, **8**, 5157-5166.
5. W. Du, A. M. Nyström, L. Zhang, K. T. Powell, Y. Li, C. Cheng, S. A. Wickline and K. L. Wooley, *Biomacromolecules*, 2008, **9**, 2826-2833.
6. K. J. Thurecht, I. Blakey, H. Peng, O. Squires, S. Hsu, C. Alexander and A. K. Whittaker, *Journal of the American Chemical Society*, 2010, **132**, 5336-5337.
7. I. Tirotta, V. Dichiarante, C. Pigliacelli, G. Cavallo, G. Terraneo, F. B. Bombelli, P. Metrangolo and G. Resnati, *Chemical Reviews*, 2015, **115**, 1106-1129.
8. M. Srinivas, A. Heerschap, E. T. Ahrens, C. G. Figdor and I. J. M. de Vries, *Trends in biotechnology*, 2010, **28**, 363-370.
9. C. K. Fu, J. Tang, A. D. Pye, T. Q. Liu, C. Zhang, X. Tan, F. Han, H. Peng and A. K. Whittaker, *Biomacromolecules*, 2019, **20**, 2043-2050.
10. O. Munkhbat, M. Canakci, S. K. Zheng, W. G. Hu, B. Osborne, A. A. Bogdanov and S. Thayumanavan, *Biomacromolecules*, 2019, **20**, 790-800.
11. M. Srinivas, P. Boehm-Sturm, C. G. Figdor, I. J. de Vries and M. Hoehn, *Biomaterials*, 2012, **33**, 8830-8840.
12. I. Tirotta, A. Mastropietro, C. Cordiglieri, L. Gazzera, F. Baggi, G. Baselli, M. G. Bruzzone, I. Zucca, G. Cavallo, G. Terraneo, F. Baldelli Bombelli, P. Metrangolo and G. Resnati, *Journal of the American Chemical Society*, 2014, **136**, 8524-8527.

13. A. T. Preslar, F. Tantakitti, K. Park, S. Zhang, S. I. Stupp and T. J. Meade, *ACS Nano*, 2016, **10**, 7376-7384.

14. D. Wilms, S.-E. Stiriba and H. Frey, *Accounts of Chemical Research*, 2010, **43**, 129-141.

15. H. Wu, T. Yin, K. Li, R. Wang, Y. Chen and L. Jing, *Polymer Chemistry*, 2018, **9**, 300-306.

16. I. N. Kurniasih, H. Liang, S. Kumar, A. Mohr, S. K. Sharma, J. P. Rabe and R. Haag, *Journal of Materials Chemistry B*, 2013, **1**, 3569-3577.

17. M. Imran ul-haq, B. F. L. Lai, R. Chapanian and J. N. Kizhakkedathu, *Biomaterials*, 2012, **33**, 9135-9147.

18. S. Abbina, S. Vappala, P. Kumar, E. M. J. Siren, C. C. La, U. Abbasi, D. E. Brooks and J. N. Kizhakkedathu, *Journal of Materials Chemistry B*, 2017, **5**, 9249-9277.

19. G. Kasza, G. Kali, A. Domján, L. Pethő, G. Szarka and B. Iván, *Macromolecules*, 2017, **50**, 3078-3088.

20. S. Roller, H. Zhou and R. Haag, *Molecular Diversity*, 2005, **9**, 305-316.

21. X. Yu, Z. Liu, J. Janzen, I. Chafeeva, S. Horte, W. Chen, R. K. Kainthan, J. N. Kizhakkedathu and D. E. Brooks, *Nature Materials*, 2012, **11**, 468.

22. M. Zieringer, M. Wyszogrodzka, K. Biskup and R. Haag, *New Journal of Chemistry*, 2012, **36**, 402-406.

23. M. Krämer, J. F. Stumbé, H. Türk, S. Krause, A. Komp, L. Delineau, S. Prokhorova, H. Kautz and R. Haag, *Angewandte Chemie International Edition*, 2002, **41**, 4252-4256.

24. K. K. Rajesh and B. D. E., *Macromolecular Rapid Communications*, 2005, **26**, 155-159.

25. O. Wagner, M. Zieringer, J. W. Duncanson, A. D. Weitz and R. Haag, *International Journal of Molecular Sciences*, 2015, **16**.

26. Y. Thomann, R. Haag, R. Brenn, R. Delto, H. Weickman, R. Thomann and R. Mülhaupt, *Macromolecular Chemistry and Physics*, 2004, **206**, 135-141.

27. Y. Li, X. Wang, H. Zhang, Y. Wang, Y. Yan, Y. Zhang and Y. Zhao, *Journal of Surfactants and Detergents*, 2014, **17**, 977-984.

28. Y. Zhang, Y. Yan, Y. Wang, Y. Li, X. Wang, H. Zhang, J. Liu and F. Wang, *Colloids and Surfaces A: Physicochemical and Engineering Aspects*, 2013, **436**, 563-569.

29. A. Berkessel, J. Krämer, F. Mummy, J.-M. Neudörfl and R. Haag, *Angewandte Chemie International Edition*, 2012, **52**, 739-743.

30. O. Wagner, J. Thiele, M. Weinhart, L. Mazutis, D. A. Weitz, W. T. S. Huck and R. Haag, *Lab on a Chip*, 2016, **16**, 65-69.

31. R. Xie, Q. Jin, Y. Zhang, Y. Yan and Y. Zhao, *Journal of Dispersion Science and Technology*, 2013, **34**, 842-846.

32. R. K. Kainthan, E. B. Muliawan, S. G. Hatzikiriakos and D. E. Brooks, *Macromolecules*, 2006, **39**, 7708-7717.

33. A. Sunder, R. Hanselmann, H. Frey and R. Mülhaupt, *Macromolecules*, 1999, **32**, 4240-4246.

34. J. Seiwert, D. Leibig, U. Kemmer-Jonas, M. Bauer, I. Perevyazko, J. Preis and H. Frey, *Macromolecules*, 2016, **49**, 38-47.

35. R. Bruni, P. Possenti, C. Bordignon, M. Li, S. Ordanini, P. Messa, M. P. Rastaldi and F. Cellesi, *Journal of Controlled Release*, 2017, **255**, 94-107.

36. C. Colombo, M. Li, S. Watanabe, P. Messa, A. Edefonti, G. Montini, D. Moscatelli, M. P. Rastaldi and F. Cellesi, *Acs Omega*, 2017, **2**, 599-610.

37. A. Sunder, R. Mülhaupt and H. Frey, *Macromolecules*, 2000, **33**, 309-314.

38. M. L. Brey and P. Tarrant, *Journal of the American Chemical Society*, 1957, **79**, 6533-6536.

39. A. T. Guseinova, A. M. Magerramov and M. A. Allakhverdiev, *Russian Journal of Organic Chemistry*, 2008, **44**, 946-949.

40. A. G. Davies, J. A. A. Hawari, B. Muggleton and M.-W. Tse, *Journal of the Chemical Society, Perkin Transactions 2*, 1981, 1132-1137.

41. D. Leibig, J. Seiwert, J. C. Liermann and H. Frey, *Macromolecules*, 2016, **49**, 7767-7776.

42. S. Desgouilles, C. Vauthier, D. Bazile, J. Vacus, J.-L. Grossiord, M. Veillard and P. Couvreur, *Langmuir*, 2003, **19**, 9504-9510.

43. C. Fu, C. Zhang, H. Peng, F. Han, C. Baker, Y. Wu, H. Ta and A. K. Whittaker, *Macromolecules*, 2018, **51**, 5875-5882.

44. K. Wang, H. Peng, K. J. Thurecht, S. Puttick and A. K. Whittaker, *Polymer Chemistry*, 2014, **5**, 1760-1771.

45. L. Nurmi, H. Peng, J. Seppälä, D. M. Haddleton, I. Blakey and A. K. Whittaker, *Polymer Chemistry*, 2010, **1**, 1039-1047.

46. D. Jirak, A. Galisova, K. Kolouchova, D. Babuka and M. Hruby, *Magnetic Resonance Materials in Physics, Biology and Medicine*, 2019, **32**, 173-185.

47. K. L. Peterson, K. Srivastava and V. C. Pierre, *Frontiers in chemistry*, 2018, **6**, 160-160.

48. M. S. Fox, J. M. Gaudet and P. J. Foster, *Magnetic resonance insights*, 2016, **8**, 53-67.

49. N. Hoshyar, S. Gray, H. Han and G. Bao, *Nanomedicine (London, England)*, 2016, **11**, 673-692.

50. G. I. Welsh and M. A. Saleem, *Nature Reviews Nephrology*, 2012, **8**, 14-21.